PROJECT TITLE: SAMPLING, ANALYSIS, AND PROPERTIES OF PRIMARY PM-2.5: APPLICATION TO COAL-FIRED UTILITY BOILERS

REPORT: FINAL TECHNICAL REPORT

REPORTING PERIOD: September 1999 – August 2002

AUTHOR: Allen L. Robinson, Spyros N. Pandis, Eric Lipsky, Charles Stanier, Natalie Anderson, Satoshi Takahama, Sarah Rees

DATE: February 2003

DOE AWARD #: DE-FG2699-FT40583

INSTITUTION: Carnegie Mellon University
Dept. of Mechanical Engineering, Scaife Hall
Pittsburgh, PA 15213
(412) 268 – 3657; (412) 268 – 3348 (fax)
e-mail: alr@andrew.cmu.edu

Disclaimer

Abstract

A dilution sampler was used to examine the effects of dilution ratio and residence time on the particulate emissions from a pilot-scale pulverized coal combustor. Measurements include the particle size distribution from 0.003 to 2.5 μm, $PM_{2.5}$ mass emission rate and PM2.5 composition (OC/EC, major ions, and elemental). Hot filter samples were also collected simultaneously in order to compare the dilution sampler measurement with standard stack sampling methodologies such as EPA Method 5. Measurements were made both before and after the bag-house, the particle control device used on the coal combustor. Measurements were made with three different coal types and a coal-biomass blend.

The residence time and dilution ratio do not influence the $PM_{2.5}$ mass emission rate, but have a significant effect on the size distribution and total number emissions. Measurements made before the bag-house showed increasing the residence time dramatically decreases the total particle number concentration, and shifts the particle mass to larger sizes. The effects of residence time can be explained quantitatively by the coagulation of the emitted particles. Measurements made after the bag-house were not affected by coagulation due to the lower concentration of particles. Nucleation of sulfuric acid vapor within the dilution was an important source of ultrafine particles. This nucleation is strongly a function of dilution ratio because of the competition between condensation and nucleation. At low dilution ratios condensation dominates and little nucleation is observed; increasing the dilution ratio promotes nucleation because of the corresponding decrease in available surface area per unit volume for condensation. No nucleation was observed after the bag house where conditions greatly favor nucleation over condensation; we suspect that the bag house removed the SO_3 in the flue gas. Exhaust SO_3 levels were not measured during these experiments.

Dilution caused the enrichment of selenium, ammonium and sulfate in the $PM_{2.5}$ emissions compared to the hot filter samples. The enrichment of selenium was independent of dilution ratio or residence time. The enrichment of ammonium and sulfate increased with increasing dilution ratio.

$PM_{2.5}$ emission profiles for four different fuels (two eastern bituminous coals, a western sub-bituminous coal, and coal-wood blend) were developed. These profiles compared well with profiles from similar coal sources, while showing unique characteristics due to differences in fuel composition.

Table of Contents

Executive Summary

In 1997 the US EPA proposed new standards for particulate matter with an aerodynamic diameter less than 2.5 μm ($PM_{2.5}$). Development of the regulatory framework necessary to meet these new standards requires improved understanding of the sources for $PM_{2.5}$. Coal-fired utility boilers are one important emission source for particulate matter. Utility boilers are a primary source for both fine particles and gaseous precursors such as SO_2 and NO_x that react in the atmosphere to create secondary aerosol. This project involved the design and construction of a state-of-the-art dilution sampler to investigate $PM_{2.5}$ emissions from a pilot scale pulverized coal combustor. This sampler simulates the dilution and cooling processes that occur when the hot combustion products leave the stack. The goal is to provide a more basic understanding of the emissions of $PM_{2.5}$ from coal-based power generation systems.

Experiments were performed to examine the effects of dilution ratio and residence time on particulate matter emissions from the Combustion and Environmental Research Facility (CERF) at the National Energy Technology Laboratory. The CERF is a pilot-scale pulverized coal combustor. The measurements focused on the effects of dilution ratio and residence time on the particle size distribution, $PM_{2.5}$ mass emissions, and $PM_{2.5}$ chemical composition. Experiments were performed with four different fuels: three different coals and a coal-biomass blend. The CERF was operated under steady conditions for these experiments to focus on the effects of sampling on PM emissions

The residence time and dilution ratio do not influence the particle mass emission rate, but can have a significant effect on the size distribution and total number emission rate. The high concentrations measured before the baghouse showed that increasing the residence time dramatically decreases the total particle number concentration, and shifts the particle mass to larger sizes. Under these conditions of high concentrations, increasing the dilution ratio increases the concentration of ultrafine particles. The effects of residence time can be explained quantitatively by the coagulation of the emitted particles; however the effects of dilution ratio are more complex because dilution ratio influences both the coagulation rate and gas-to-particle conversion.

Filters samples were collected before and after the baghouse for determination of mass emission rates and chemical composition. Hot filter samples were collected in parallel with the diluted samples in order to compare the effects of dilution sampling to standard stack sampling protocols such as EPA Method 5. An important issue is the effect of sampling on measurements of trace metals that are used as atmospheric tracers for coal fired combustion in source-receptor models. Species that are still semi-volatile at the exhaust temperature will pass through the hot filter as a gas, but undergo gas-to-particle conversion once the exhaust is cooled and diluted. The results show that selenium is enriched in the diluted samples compared to the hot filter samples. For the conditions of these experiments this enrichment was independent of dilution ratio and residence time.

Introduction

Ambient particulate matter (PM) is a complex mixture of multi-component particles whose size distribution, composition, and morphology can vary significantly in space and time. (Seinfeld and Pandis 1998) Atmospheric PM range in size from a few nanometers to tens of micrometers. Major PM components include sulfates, nitrate, ammonium, and hydrogen ions; trace elements (including toxic and transition metals); organic material; elemental carbon (or soot); crustal components and water. In 1997 the U.S. Environmental Protection Agency (EPA) promulgated new standards to address ambient air concentrations of PM with an aerodynamic diameter of 2.5 micrometers ($PM_{2.5}$) because of concerns over human health effects associated with fine atmospheric particles. The EPA also proposed regional haze regulations for pristine areas in 1997; fine PM is the single greatest contributor to visibility impairment in these areas. Fine PM also plays an important role in climate forcing because of their ability to scatter and absorb light and also because they act as cloud condensation nuclei. (Seinfeld and Pandis 1998) To reduce the uncertainties regarding the effects of fine PM on human health, visibility and climate, it is necessary to improve our understanding of physical and chemical properties of atmospheric particles including their size distribution, their number concentration, and their composition. These properties often depend strongly on the source of the PM. PM is emitted directly from sources (primary PM) and is also formed in the atmosphere from reactions of gaseous precursors (secondary PM). Coal-fired utility boilers are a source for both primary PM and gaseous precursors that react in the atmosphere to create secondary PM. This report examines the size distribution and composition of primary PM emissions from coal combustion.

Characterizing $PM_{2.5}$ emissions from combustion systems such as coal boilers is a difficult problem because of the high temperatures and moisture content of exhaust gases. Upon exiting the stack the combustion products are rapidly cooled and diluted with ambient air, during which time processes such as coagulation, condensation, and nucleation change the size and composition of the PM emissions. Measurements made in plumes using aircraft and at downwind ground sites provide clear evidence that PM emissions from a power plant are altered as the plume mixes with the ambient air (Cantrell and Whitby 1978; Whitby, Cantrell et al. 1978; Gillani, Kohli et al. 1981; Luria, Olszyna et al. 1983; Hildemann, Cass et al. 1989; Kim, Hopke et al. 1989; Ondov, Choquette et al. 1989; Mueller and Imhoff 1994).

Dilution sampling is a technique that has been developed to examine the influence of rapid cooling and dilution on PM emissions from combustion systems (Hildemann, Cass et al. 1989; England, Toby et al. 1998). A dilution sampler rapidly mixes hot exhaust gases with a specified amount of conditioned air and allows for processes such as nucleation, condensation, and coagulation to occur. Although a dilution sampler cannot simulate the complexity of actual plume mixing (Builtjes and Talmon 1987), it provides a better estimate of particulate emissions at ambient conditions than traditional hot-filter methods such as EPA Method 5. Dilution sampling also allows the use of more advanced aerosol instrumentation that is not compatible with the high temperature and moisture content of stack exhaust. Finally, dilution sampling allows systematic examination of the

effects of dilution on PM emissions in order to better understand the transformations that occur in plumes and to evaluate theoretical models developed to simulate power plant plumes (Damle, Ensor et al. 1984; Mueller and Imhoff 1994; Kerminen and Wexler 1995; Meng, Karamchandani et al. 2000).

Although dilution samplers have been used to characterize emissions from combustion systems such as coal boilers, relatively little research has been reported on the potential effects of sampling conditions (e.g. dilution ratio and residence time) on the measurements. Recent research by Lipsky et al. (2002) illustrates how the dilution ratio and residence time dramatically alter measurements of the particle size distribution and number emissions in coal combustion products. Similar results have been reported for diesel engines (Abdul-Khalek, Kittelson et al. 1999). Eatough et al. (1996) report that particulate lead, arsenic and selenium concentrations in diluted coal combustion exhaust are sensitive to residence time. Understanding the effects of sampling conditions is critical in order to interpret measurements made with a dilution sampler and to optimize sampler design.

The comparability between dilution sampling and standard stack sampling techniques such as EPA method 5 needs to be established because the majority of published emission profiles, such as those found in the EPA SPECIATE database, are based on traditional stack sampling techniques. Current dilution samplers are more cumbersome to operate than techniques like EPA method 5; under what conditions is this added complexity justified to provide insight into the emissions? Hildemann et al. found that a dilution sampler collected between 7 and 16 times more organic aerosol than the EPA Method 5 procedures for a distillate oil-fired industrial boiler. Such a comparison has not been reported for a coal combustion source.

This report aims to improve our understanding of the influence of dilution processes on $PM_{2.5}$ emissions from coal-fired boilers. A dilution sampler was used to characterize the $PM_{2.5}$ emissions both upstream and downstream of a bag house on a pilot-scale pulverized coal combustor. Measurements of particle size distributions from 0.003 μm – 3 μm were made for a range of dilution ratios and residences times; these data are compared to predictions from nucleation theory to investigate the influence of dilution ratio on new particle formation. Filter samples of $PM_{2.5}$ were also collected at different dilution ratio and residence times for gravimetric and composition analysis. These results are compared to hot filter samples to examine the effects of dilution sampling on $PM_{2.5}$ composition and mass emission rates.

Experimental

Experiments to examine the effects of dilution sampling were performed on the exhaust of the Combustion and Environmental Research Facility (CERF) at the Department of Energy National Energy Technology Laboratory. The CERF is a pilot-scale pulverized coal combustor designed to simulate the time-temperature history of a commercial coal boiler. At full load it consumes 20 kg of pulverized coal per hour,

roughly 150 kW when burning a US bituminous coal. Coal is injected through a swirl-stabilized burner at the top of a 3-m tall and 45-cm diameter refractory lined combustion zone. Combustion products then flow into a horizontal convective section, through two flue gas coolers, heat-traced piping, and into a bag-house. Sampling was performed both before and after the bag-house, but not at both locations simultaneously. The CERF was operated under the same nominal conditions for all of these experiments in order to examine the effects of sampling conditions and fuel properties on emissions.

Experiments were performed while firing three different coals and a coal-wood blend; Table 1 presents results from standard analyses of the different fuels. The coals represent a range of common utility and industrial fuels: Prater Creek Coal is an eastern bituminous coal with low sulfur and ash content; Black Thunder Coal is a low sulfur, high calcium sub-bituminous coal from the Powder River Basin; and Bailey Mine Coal is a high sulfur, Pittsburgh seam bituminous coal. The coal samples were fired in pulverized form, commercial grind, 70% through 200 mesh. The wood fuel is ground pallets, and was included to examine the effects of coal-biomass cofiring on $PM_{2.5}$ emissions. The wood was milled finely enough to pass through a 1-mm mesh, and blended with Prater Creek Coal (55% wood, by weight) before firing.

Table 1: Fuel composition.

	Prater Creek	Bailly Mine	Powder River Basin: Black Thunder	Ground Pallets (PA)
Ultimate Analysis, wt%				
Hydrogen	5.4	5.06	6.00	4.80
Carbon	78.3	76.47	60.02	1.00
Nitrogen	2.3	1.52	0.90	0.22
Sulfur	0.8	1.82	0.43	0.10
Oxygen	8.4	7.46	25.35	36.65
Ash	4.7	7.67	7.30	15.83
Heating Value (Btu/lb)	14167	13635	10028.2	6737
Percent as Oxides, wt%				
SiO_2	38.40	48.90	36.22	14.73
$Al2O_3$	25.00	23.75	17.52	4.15
Fe_2O_3	22.50	17.09	5.69	10.49
TiO_2	1.00	1.07	1.32	8.78
P_2O_5	0.10	0.36	0.94	0.00
CaO	3.80	2.78	18.20	37.37
MgO	2.10	0.77	3.63	6.27
Na_2O	0.30	0.59	1.43	11.68
K_2O	2.20	1.73	0.94	3.17
SO_3	4.60	2.61	n/a	n/a
MnO_2	n/a	0.04	n/a	n/a

Figure 1 shows a schematic of the Carnegie Mellon University (CMU) dilution-sampling system (henceforth referred to as the CMU sampler) developed for this investigation. The design is based on the Caltech dilution sampler (Hildemann, Cass et al. 1989), with improvements that allow for the independent control of dilution ratio and residence time to allow investigation of the effects of these parameters on emissions.

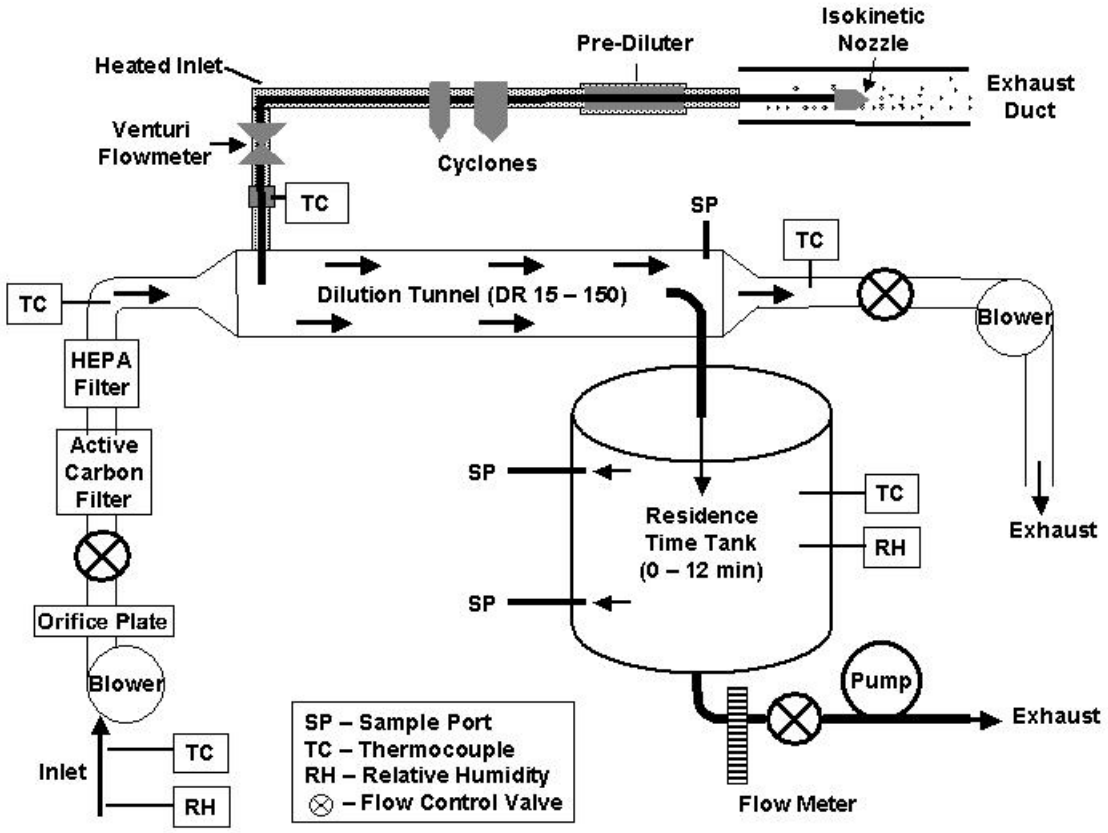

Figure 1: Schematic of the CMU dilution sampler

The CMU sampler consists of three major components: the sample inlet line, the dilution tunnel, and the residence time tank. Combustion products are drawn isokinetically from the exhaust duct through an inlet line, $PM_{2.5}$ cyclone, and a venturi flow meter, all heated to the exhaust temperature. The combustion products are then turbulently mixed in the dilution tunnel, a 15-cm-diameter, 2.3-m-long tube, with ambient air that has passed through a HEPA filter and an activated carbon bed. The flow rate of both the dilution air into the tunnel and the combustion products through the inlet line are directly measured. At the end of the dilution tunnel, a slipstream of the diluted mixture is drawn continuously through the residence time tank. The residence time tank has a separate flow control system, which allows independent control of the residence time and the dilution ratio. Sampling ports for aerosol characterization instrumentation and filter packs are located at the end of the dilution tunnel and at various locations on the residence time tank. All of the parts of the sampler in contact with the exhaust sample and the diluted mixture are made of stainless steel with Teflon gaskets. A more detailed

description of the sampler can be found in a previous publication (Lipsky, Stanier et al. 2002).

Experiments were conducted to examine the effects of dilution ratio and residence time on the PM size distribution, $PM_{2.5}$ composition, and $PM_{2.5}$ mass emission rate while the CERF was operated at constant conditions. For each experiment, the flows through the dilution sampler are set to achieve the desired dilution and maximum residence time. The system is then operated for a period of one- to two-hours to allow for multiple air changes to occur within the residence time tank before collection of samples for analysis. After this equilibration period, samples of diluted exhaust are drawn simultaneously through multiple ports at the end of the dilution tunnel and at various locations on the residence time tank. The sampler design allows for simultaneous sampling at three different residence times: the ports at the end of the dilution tunnel are considered zero residence time, and the ports half-way and at the end of the residence time tank collect ½ and full residence time samples, respectively. This approach helps isolate the effects of residence time from the inherent variations in fuel quality and combustor operating conditions. Tracer experiments were performed to characterize the sample transit time through the residence time tank as detailed in previous work (Lipsky, Stanier et al. 2002). Samples at different dilution ratios cannot be collected simultaneously. Therefore, a series of experiments were performed to examine the effects of dilution ratio; between each experiment the dilution sampler flows are adjusted to the new set point and the system is allowed to reach equilibrium.

The dilution ratio is defined as

$$DR = \frac{Q_{sample} + Q_{dilution}}{Q_{sample}} \quad (1)$$

where Q_{sample} is the measured flowrate of the combustion products through the inlet line, and $Q_{dilution}$ is the measured flow rate of conditioned dilution air into the tunnel. All flows are defined at standard conditions (25 °C and 1 atmosphere). Results are reported on a unit exhaust volume basis of the pilot-scale by multiplying the measured concentration in the diluted exhaust by the dilution ratio.

Measurements of particle size distributions from 0.003 μm – 3 μm were made using sizing instrumentation connected to the sample ports on the dilution tunnel and residence time tank. One Scanning Mobility Particle Sizer (SMPS) measures particles between 0.003 μm and 0.075 μm (TSI model 3085 Electrostatic Classifier with a TSI model 3025 CPC). A second SMPS measures particles from 0.015 μm - 0.65 μm (TSI model 3081 Electrostatic Classifier with a TSI model 3010 CPC). An Aerodynamic Particle Sizer (TSI APS) measures particles in the range of 0.5 μm – 3 μm, overlapping with the second SMPS (TSI model 3320). Two neutralizers are used in series before both of the SMPS analyzers to ensure a known charge on the particles. Further dilution of the sample flow was required under certain conditions to lower concentrations of the particles below maximum detection levels of the CPC.

Filter samples were collected to determine the $PM_{2.5}$ mass emission rate and $PM_{2.5}$ composition (47-mm, 2-μm Teflo filters, Gelman Corp). Two Teflon filters were collected at each residence time: one filter was used for gravimetric analysis and ion chromatography; the second filter was used for elemental analysis via inductively couple plasma mass spectroscopy (ICP-MS). A series of handling and dynamic blanks were collected during the experiments; all filter measurements are corrected for appropriate blanks. During some experiments, $PM_{2.5}$ samples were also simultaneously collected on Teflon filters using a hot filter sampler similar to EPA Method 5, in which combustion products were sampled isokinetically and then passed through a $PM_{2.5}$ cyclone and filter pack, all heated to the exhaust temperature.

$PM_{2.5}$ mass emission rates were determined based on pre- and post-sampling filter mass. All gravimetric analysis was performed in a temperature (21-23 °C) and relative humidity (30-40%) controlled glove box following standard EPA protocols. The filters were allowed to equilibrate within the glove box for at least 24-hours before being weighed.

$PM_{2.5}$ elemental composition was determined using inductively coupled plasma mass spectrometry (ICP-MS). Exposed Teflon filters were digested in 2.5 mL of redistilled nitric acid (GFS Chemicals, Inc., Powell, OH), and 7.5 mL of distilled, de-ionized water in a closed vessel in a MARS5 microwave (CEM Corp., Matthews, NC), which heated the samples to 180^{o}C over a 10-minute period, followed by a 10-minute hold at 180^{o}C. The digested samples were then cooled and diluted by factors of 2, 10, and 100, and a multi-element internal standard (SPEXCertiprep, Metuchen, NJ) was added to each sample to decrease matrix effects. Digested samples were analyzed for 21 elements using an HP 4500 ICP-MS. The ICP-MS was calibrated with external standards (SPEXCertiprep), and microwave-digested samples of the NIST SRM 1648 Urban Particulate Matter was analyzed to validate filter sample analysis results.

$PM_{2.5}$ ion concentrations were determined using ion chromatography. Exposed Teflon filters were digested in 2 mL of Methanol Optima (CAS 67-56-1) and immersed in 28mL of distilled, deionized water (DDW) with a resistivity of 18.2 mΩ-cm. The filters were then sonicated for an hour and kept cold (<5^{o}C) where they were allowed to sit for twelve hours. A fraction of this filter extract was pipetted and combined with DDW to prepare 25 mL of solution for analysis. Five mL of this solution was drawn into a new disposable syringe (Becton Dickinson, PN 309645) and used to rinse the syringe and filter (PALL-Gelman Laboratory Acrodisc, PN 4583T) to remove particles insoluble in water. Two aliquots of 5 mL each were apportioned into the ion chromatography autosampler vials (DIONEX, PN 038009) with filter caps for replicate analyses. Each sample was analyzed for sodium, ammonium, potassium, magnesium, calcium, chloride, nitrite, nitrate, and sulfate by simultaneous injection into a DIONEX DX-120 and DX-600.

A limited number of samples were collected on quartz fiber filters (Gelman 47 mm, Tissuquartz 2500 QAO-UP) for organic and elemental carbon analysis. Prior to sampling, the quartz filters were baked at 550 °C in air for a minimum of 4 hours to minimize residual carbon. The quartz filters were analyzed after sampling using a Sunset

Laboratories Thermal Optical Transmittance (TOT) OC/EC analyzer following the NIOSH 5040 protocol.

The effects of dilution on $PM_{2.5}$ composition are evaluated using an enrichment factor (EF). The enrichment factor is defined as

$$EF_i = \frac{y_{i,dilute}}{y_{i,hot}} \qquad (2)$$

where $y_{i,dilute}$ and $y_{i,hot}$ is the $PM_{2.5}$ mass fraction of element or species i in the diluted and hot sample, respectively. An enrichment factor greater than one indicates that a species is enriched in the diluted sample compared to the hot sample; an enrichment factor equal to one indicates no difference between the hot and dilution sampling methods for that species.

Data Analysis

Two types of analysis are performed to examine the changes in the size distribution with residence time and dilution ratio. First, a coagulation model is used to simulate the changes over time of the particle size distribution within the residence time tank to better understand the effects of dilution and residence time on the measured size distributions. The model describes the evolution of the aerosol size distribution of an isolated air parcel with time due to coagulation due to Brownian motion. The initial condition for the calculation is a three-mode lognormal distribution fit to the measurements of the particle size distribution made at the end of the dilution tunnel (zero residence time). More details on the model can be found in a previous publication (Lipsky, Stanier et al. 2002).

A second model is used to examine the effects of dilution on nucleation within the dilution tunnel. The rapid cooling of the combustion products within the dilution tunnel causes SO_3 in the exhaust to react with water to form sulfuric acid, which then undergoes rapid gas-to-particle conversion by either condensing on to existing particles or nucleating to form new particles. The binary nucleation of sulfuric acid and water vapor is a highly nonlinear process that depends strongly on the temperature, relative humidity, and acidity. Absolute nucleation rates are difficult to predict; instead we use the framework of Kerminen and Wexler {, 1995 #16} to predict the conditions under which nucleation is expected to occur. Nucleation is expected to occur when the concentration of $H_2SO_4(g)$ exceeds a critical concentration,

$$C_{crit} = 0.16\exp(0.1T - 3.5rh - 27.7) \qquad (3)$$

where the critical concentration, C_{crit}, is in $\mu g\ m^{-3}$, T is the temperature in Kelvin, and rh is the relative humidity, scaled 0-1. This critical concentration is the concentration of $H_2SO_4(g)$ at which for a given temperature and relative humidity the nucleation rate is 1 nucleus s^{-1} cm^{-3}. If the sulfuric acid concentration in the tunnel exceeds this critical concentration than nucleation is expected to occur.

Predicting the conditions under which nucleation is expected to occur requires knowledge of the sulfuric acid concentration within the dilution tunnel and the corresponding critical concentration at tunnel conditions. Using a mass balance we predict the change in concentration of sulfuric acid with time as an air parcel passes through the tunnel accounting for the effects of dilution and condensation.

$$\frac{dC}{dt} = -C\left(\frac{1}{\tau_c} + \frac{1}{\tau_d}\right) \tag{4}$$

where τ_c^{-1} is the condensation rate onto pre-existing particles, and τ_d^{-1} is the dilution rate due to mixing. We assume that no production of H_2SO_4 occurs within the tunnel because of the short residence time in the dilution tunnel and the extremely low radical levels in the exhaust.

The condensation rate is defined as,

$$\tau_c^{-1}(t) = \sum_i \frac{2\pi D\, d_{p,i}\left(\frac{N_i}{1+DR(t)}\right)}{1+\frac{2\lambda}{\alpha\, d_{p,i}}} \tag{5}$$

where D is diffusivity of H_2SO_4 in air, $d_{p,i}$ is the geometric mean diameter of particles in section i, N_i is the undiluted concentration of particles in section i, DR(t) is the dilution ratio of the parcel with time, λ is the mean free path of air, and α is the mass accommodation coefficient. Equation (5) assumes that the concentration of sulfuric acid at the particle surface is zero. For the calculations we use a diffusivity of 0.1cm^2 sec^{-1} and an accommodation coefficient of 0.05 based on work by Van Dingenen and Raes (1991). The particle concentration, N_i, is determined from the measured particle size distribution at the end of the tunnel.

The sample and dilution air are mixed by turbulence within the tunnel. The mixing rate, τ_d^{-1}, inside the tunnel was determined by performing mixing experiments using carbon dioxide as a tracer. The experiment involved injecting a pure stream of carbon dioxide at 150 °C through the sample inlet line at 20 lpm (a typical inlet condition). The radial distribution of carbon dioxide concentration was then measured at 12 cm increments along the dilution tunnel.

Figure 2 presents results from several mixing experiments conducted at different dilution ratios. Since the mixing rate varies with dilution ratio, results are presented as a function of the normalized axial distance, which is the axial distance from the inlet point normalized by the distance required for complete mixing. Figure 2 shows that by plotting the mixing rate as a function of normalized distance the results from the experiments conducted at different dilution ratios fall on the same set of curves. As expected, the mixing rate varies radially with the most rapid mixing occurring near the tunnel wall, and

the slowest mixing occurring along the tunnel centerline. Nucleation is expected to first occur where the mixing is most rapid; therefore we use the maximum mixing rate for the nucleation calculations. For implementation in the model a curve was fit to the maximum mixing rate data as indicated by the solid line in Figure 2.

The sulfuric acid concentration of an air parcel as it passes through the dilution tunnel is determined by numerically solving equation (4). The concentration of H_2SO_4 at the inlet to the dilution tunnel is determined based on an estimate of the SO_3 level in the exhaust. The SO_3 level is assumed to be 3% of the measured exhaust SO_2 (Flagan et al. 1988), and that all of this SO_3 is converted to H_2SO_4 at the inlet to the tunnel. In order to evaluate the critical concentration using equation (3) for a given location within the tunnel, the temperature and relative humidity are calculated from using the measured temperature and moisture content of the combustion products and dilution air at the tunnel inlet, the mixing rate (Figure 2), and assuming that mixing occurs adiabatically.

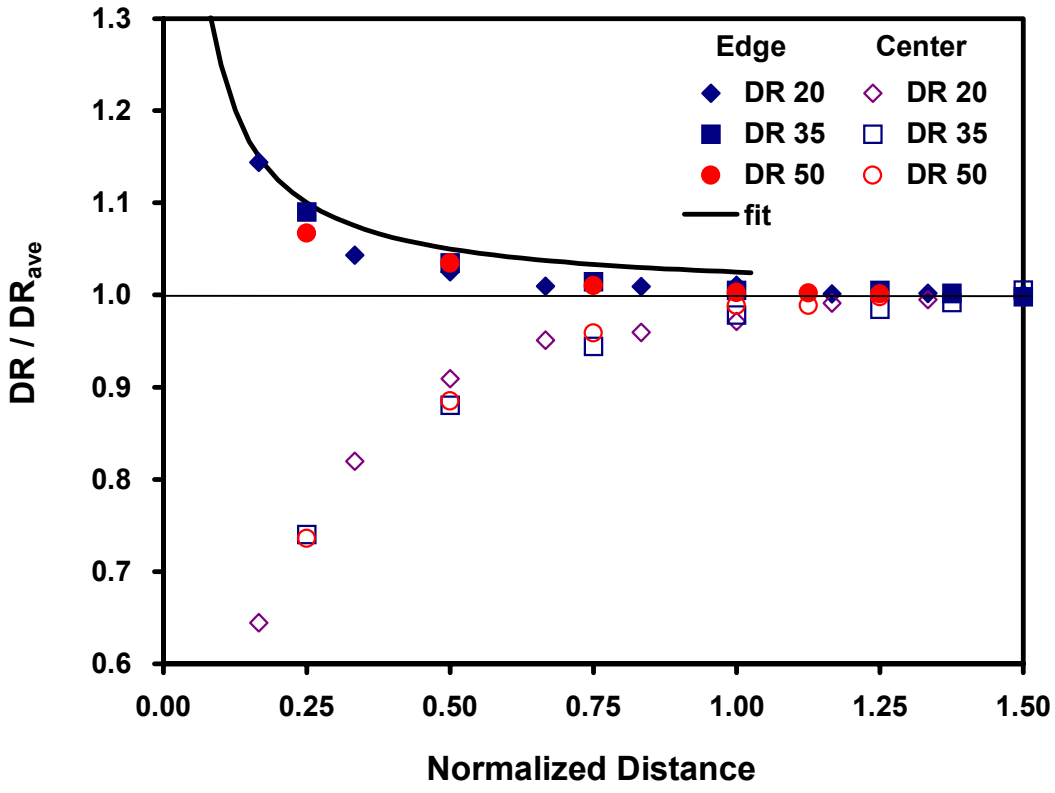

Figure 2. Mixing rate as a function of normalized distance along the dilution tunnel determined from the carbon dioxide tracer experiments. Results are presented for the measured dilution ratio along the tunnel centerline (solid symbols) and adjacent to the wall (open symbols) normalized by the average dilution ratio at three different dilution ratios. The mixing rates for other radial locations fall between these bounds. The line is a fit to the data used as the maximum mixing rate within the tunnel for the nucleation calculations. A normalized distance of 1 corresponds to the location where the combustion products and dilution air are well mixed.

Results and Discussion

Size Distributions:

Typical size distributions measured before and after the bag-house are shown in Figure 3. Before the bag house three modes are seen in the $PM_{2.5}$ size distribution with peaks at 10 nm, 50-100 nm, and 1.5 μm; after the baghouse only the two larger modes are present. The 50-100 nm mode is formed from trace metals that are volatilized by the high temperatures of the combustion process (Linak and Wendt 1994; Lighty, Veranth et al. 2000). The supermicron mode dominates the volume distribution and is residual fly ash (Lighty, Veranth et al. 2000). The 10 nm mode dominates the number distribution and is formed from the nucleation of sulfuric acid occurring in the dilution tunnel (Damle, Ensor et al. 1984; Flagan and Seinfeld 1988; Mueller and Imhoff 1994); after the baghouse, this nucleation mode (~10 nm) is not observed.

In previous work (Lipsky, Stanier et al. 2002), we reported on the effects of residence time and dilution ratio on the size distributions before the bag house. We found changes in the size distribution with residence time could be quantitatively explained by coagulation due to Brownian motion. We also found changes in the size distribution with dilution ratio; increasing the dilution ratio increases the particle number, especially in the ultra-fine 10-nm mode. This report focuses on comparing the before the bag house results with measurements after the bag house, and applying nucleation theory to help explain the effects that dilution ratio has on the size distribution.

Figure 4 shows the effects of residence time on the size distribution both before and after the bag-house. The dramatic changes in the size distribution before the bag house (Figure 4a) are due to coagulation (Lipsky, Stanier et al. 2002). No changes in the particle number distribution with residence time were seen after the bag-house.

Evaluation of the characteristic time for coagulation can be used to identify conditions where coagulation will be important. The characteristic time for coagulation of a monodisperse aerosol is

$$\tau_c = \frac{2}{KN_o} \tag{6}$$

where K is the coagulation coefficient, which is a function of particle size, and N_o the number concentration within the dilution tunnel. When sampling before the bag house at a dilution ratio of 70, the characteristic times for coagulation of the 10 nm and 50 nm modes are 48 and 370 seconds, respectively. These times are comparable to the residence time and therefore significant changes due to coagulation are expected. Increasing the dilution ratio slows coagulation; however, before the bag house, coagulation rates were significant even at the highest dilution ratios because of the extremely high number concentrations. After the bag-house the particle number concentrations are much lower which results in much slower coagulation rates. The characteristic time for coagulation of the 50-nm mode is on the order of 36,000 seconds after the bag house for at a dilution

ratio of 70. Under these conditions coagulation is not expected to occur, which is consistent with the results.

Figure 5 compares the total number emissions before and after the bag house as a function of residence time. Before the bag house, coagulation dramatically reduces the total particle number with time. After the bag house, the total number emissions do not vary with residence time. The observed trends agree well with the predictions of the coagulation model, as shown in Figure 5. This agreement suggests that the main process occurring within the residence time tank for these conditions is Brownian coagulation of the emitted particles.

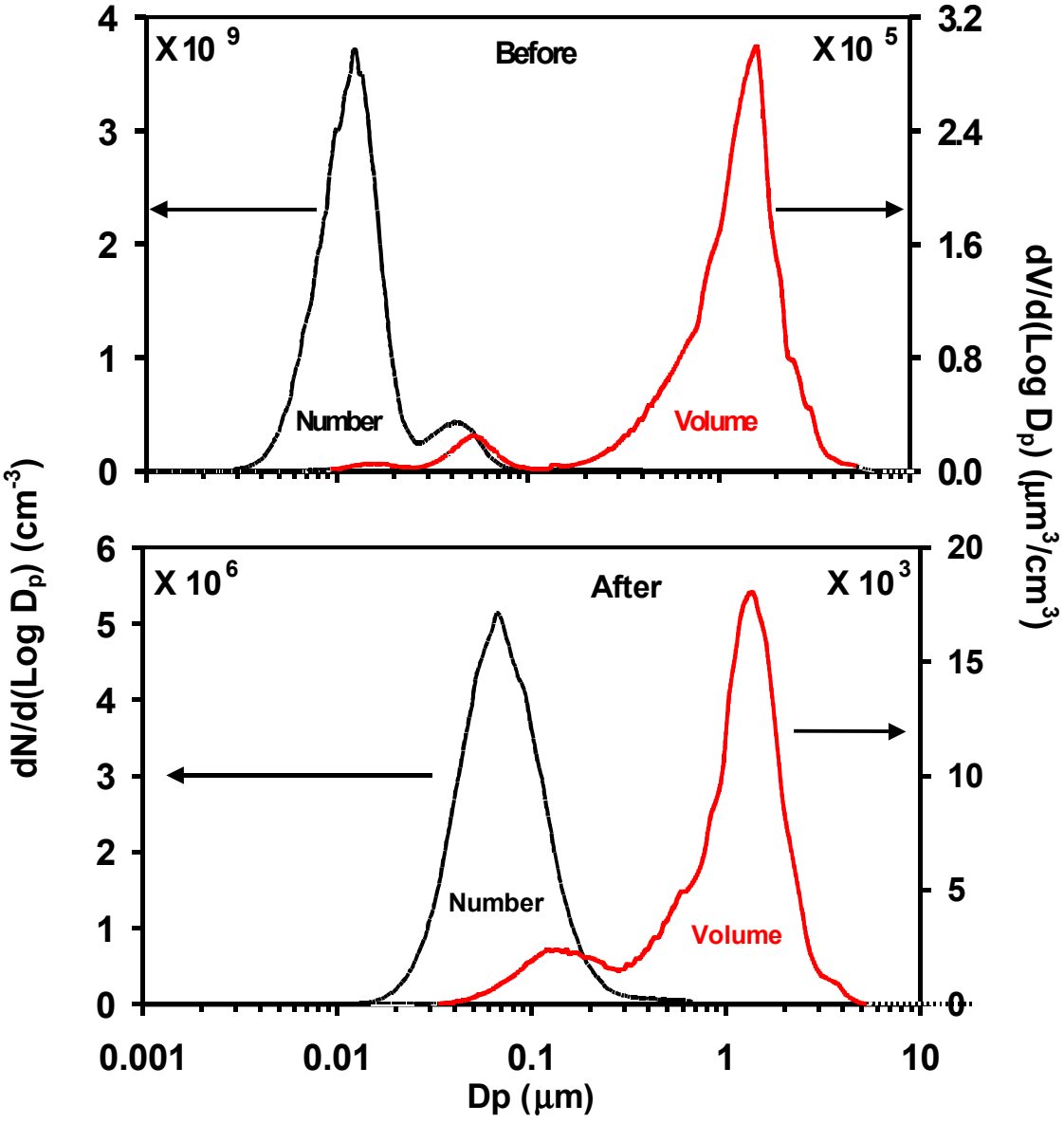

Figure 3: Typical number and volume distributions before and after the baghouse. Size distributions were measured while operating the CERF under the same condition firing Prater Creek Coal.

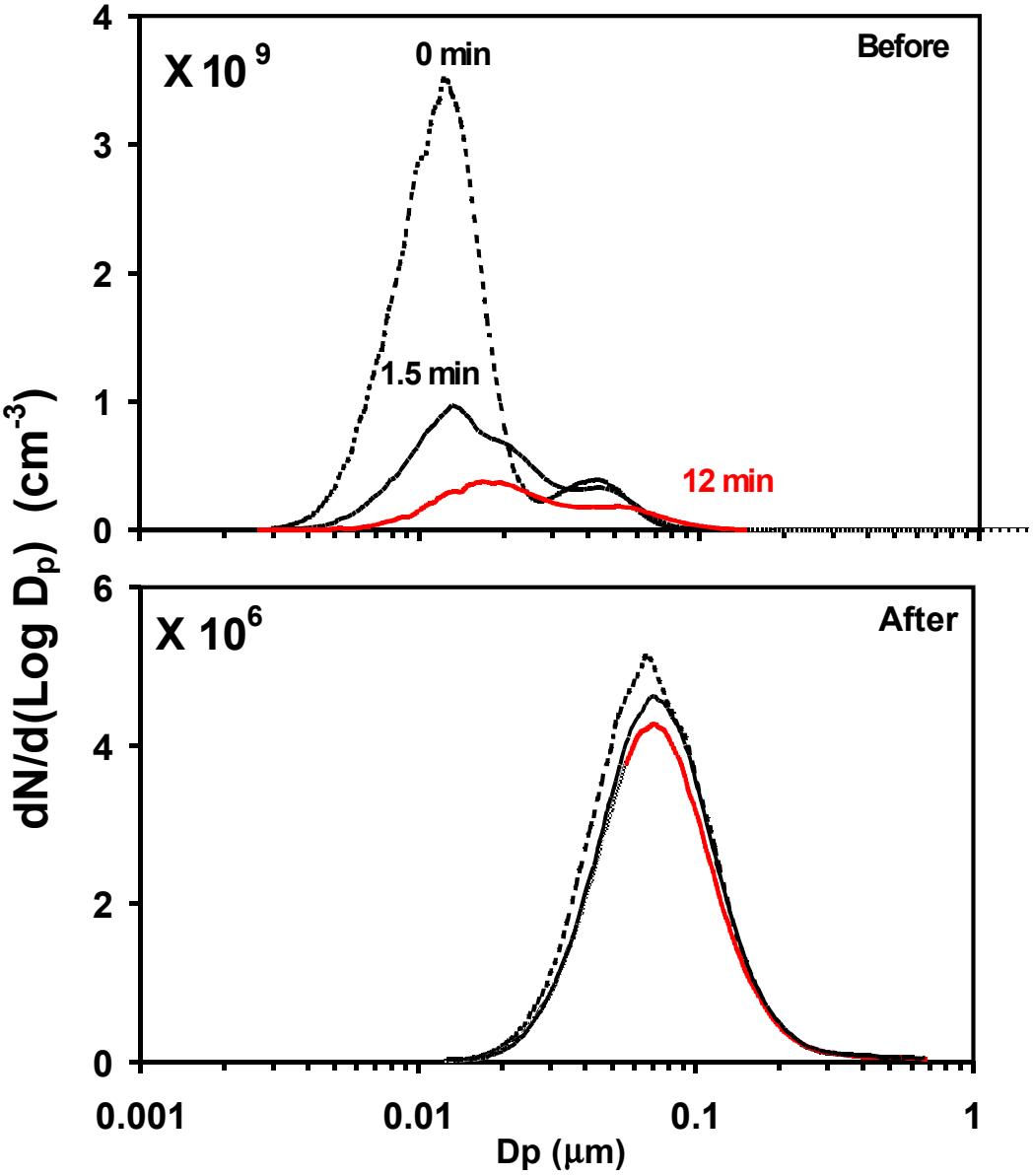

Figure 4: Particle size distribution measured at different residence times before and after the bag house while firing Prater Creek Coal. The zero-time number distribution is measured at the end of the dilution tunnel and before the mixture enters the residence time tank. The distribution at 1.5 and 12 minutes are both measured using ports in the residence time tank. The experiments were performed at a dilution ratio of 70.

The effects of dilution ratio on the number size distribution are shown in Figure 6. Changing the dilution ratio dramatically alters the measured size distribution before the bag house. Increasing the dilution ratio increases the particle number, especially in the ultrafine 10-nm mode. Changing the dilution ratio does not effect the size distribution of particles greater than 1 µm. After the bag house there are no significant changes in the size distribution with dilution ratio.

Figure 7 plots the total number emissions as a function of dilution ratio. Before the bag house, the total numbers of particles increases with dilution ratio. This trend can be largely attributed to the effects of dilution ratio on the ultrafine 10-nm mode. After the bag house, the total number of particles stays relatively constant, and roughly 2 orders of magnitude smaller than emissions before the bag house.

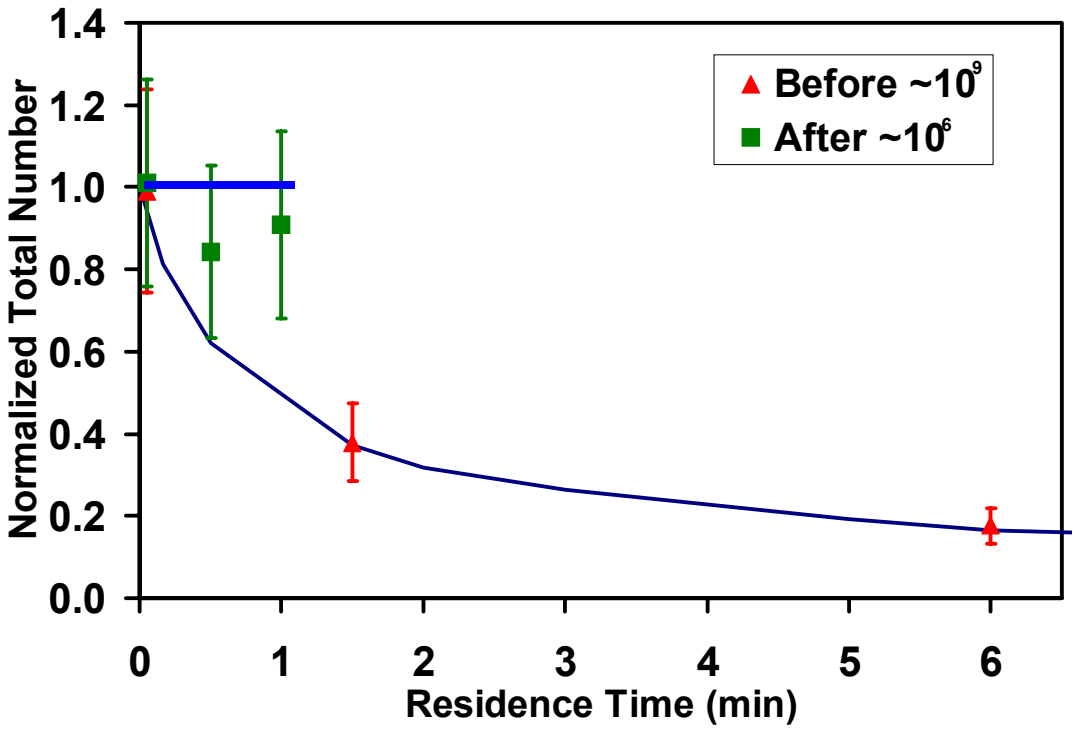

Figure 5: Change in total number emissions with residence time measured while firing Prater Creek Coal. Points are measured data with standard deviations. The lines are total number predicted by the coagulation model. The dark blue line is simulated from zero residence time conditions observed before the bag house. The light blue line is simulated from zero residence time conditions observed after the bag house.

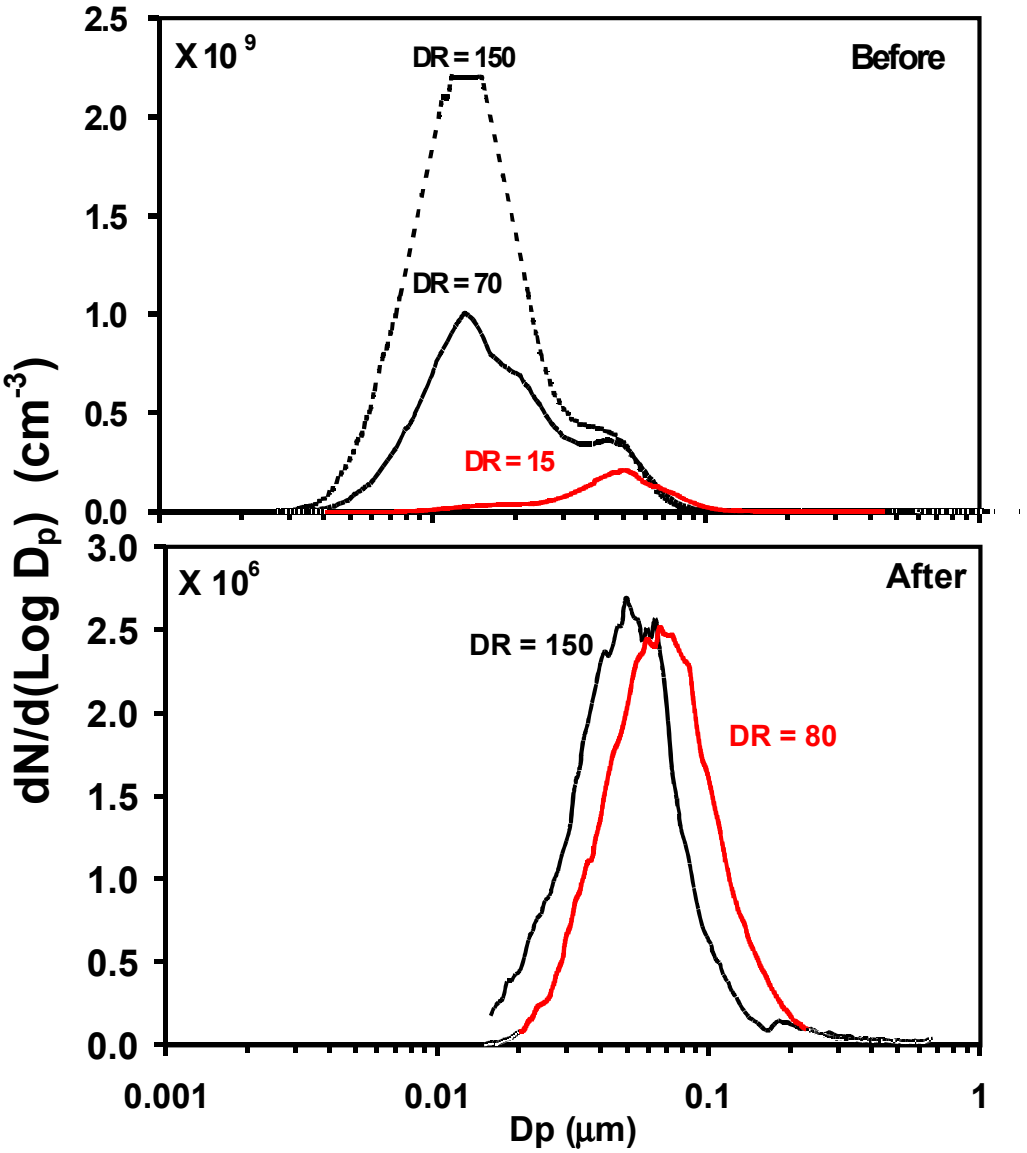

Figure 6: Particle number size distribution measured at different dilution ratios while firing Prater Creek Coal: (a) before the bag house (dilution ratios of 15, 70 and 150 at a residence time of 1.5 minutes); (b) after the bag house (dilution ratios of 80 and 150 at a residence time of 0 minutes).

The changes in the 10-nm mode with dilution ratio observed before the bag house (Figure 6) suggest that dilution ratio effects new particle formation. Upon entering the dilution tunnel, the combustion products are rapidly diluted and cooled causing SO_3 to react with H_2O to create H_2SO_4, sulfuric acid. The rapid cooling of the combustion products creates a super-saturation of sulfuric acid. Whether or not this material condenses or nucleates to create new ultrafine particles depends on the available particle surface area.

Figure 8 plots the ratio of the sulfuric acid concentration calculated with equation (4) and the critical concentration calculated with equation (3) as a function of the normalized distance along the tunnel. When this ratio exceeds one, nucleation is expected to occur. Calculations are shown for three scenarios: before the bag house low dilution ratio, before the bag house high dilution ratio, and after the bag house. Inputs for these calculations are based on the measured experimental conditions.

Figure 7: Effects of dilution ratio on the total number of measured particles. Results are from size distributions measured at 1.5 minute residence time.

The model predictions shown in Figure 8 indicate that, before the bag house, nucleation depends on the dilution ratio. At a dilution ratio of 15, the critical ratio never exceeds 1 and nucleation is not expected to occur. At a dilution ratio of 75, the critical ratio exceeds 1 and nucleation is expected occur. These predictions are consistent with the size distribution measurements made before the bag house shown in Figure 6a. The absence of a 10-nm mode in the dilution-ratio-15 size distribution indicates that nucleation is not occurring under these conditions. A substantial 10-nm mode is observed at higher dilution ratios indicating significant nucleation. This trend is due to effect of dilution ratio on the available particle surface area, which, in turn, alters the condensation rate of H_2SO_4. At low dilution ratios, the available particle surface area per unit volume is high, condensation occurs rapidly, and the critical concentration is not exceeded. Increasing the dilution ratio decreases the available surface area, slowing condensation, an allowing nucleation to occur. Similar observations regarding the

complex relationship between dilution ratio and aerosol size distribution have been made in studies of diesel exhaust particles (Abdul-Khalek, Kittelson et al. 1999).

Conditions after the bag house favor nucleation because of the much lower available surface area. For example, the calculations in Figure 8 indicate that even at low dilution ratios the critical ratio exceeds one and nucleation is expected to occur after the bag house. However, after the bag house a 10-nm mode was not observed indicating that nucleation did not occur (Figure 6b). The model calculations shown in Figure 8 are based on an assumed exhaust SO_3 concentrations; the absence of nucleation after the bag house is likely due to the bag removing SO_3 from the exhaust. Measurements were not performed to validate this hypothesis.

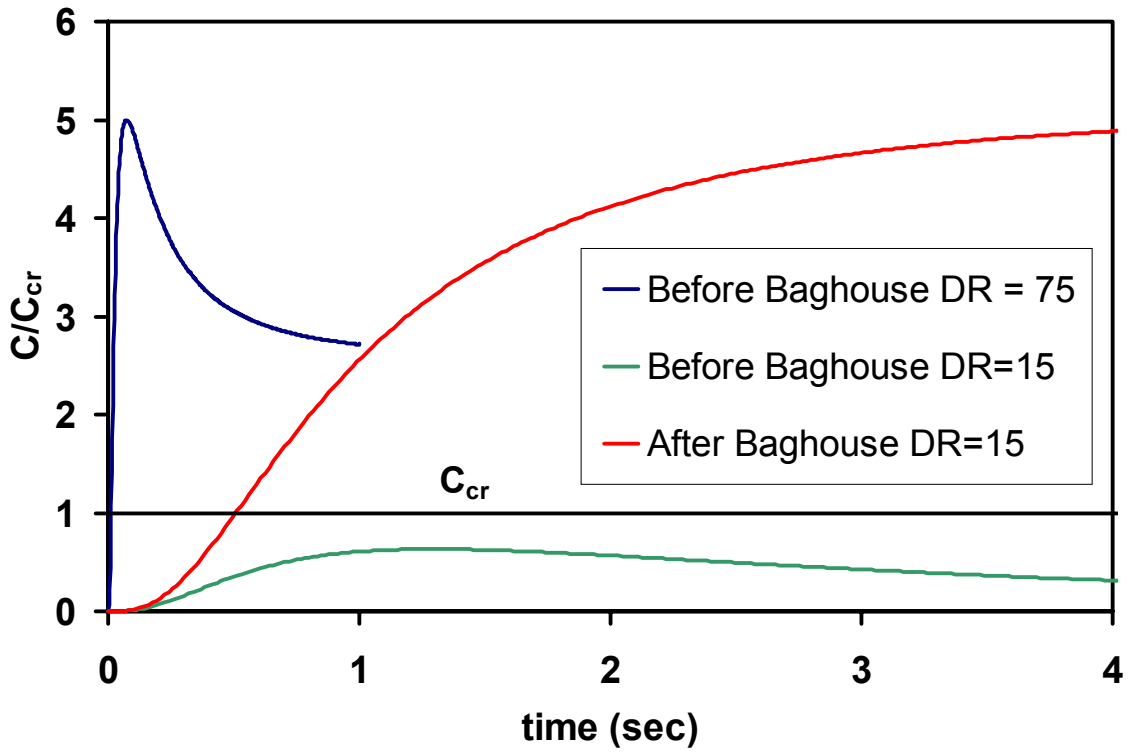

Figure 8: Nucleation predictions based on inlet conditions to the dilution tunnel. If the critical ratio exceeds 1, nucleation is favored. The blue and green lines are model predictions from inlet conditions observed before the baghouse with high dilution (DR=75) and low dilution (DR=15) respectively. The red line predicts nucleation after the baghouse under inlet conditions observed at low dilution (DR=15). Nucleation was not observed after the baghouse.

$PM_{2.5}$ Mass Emissions:

Table 2 lists average measured mass emissions rates measured using the dilution sampler and a hot filter sampler while firing Prater Creek coal. The before and after the bag house results are the average of 5 and 2 tests, respectively. Within experimental uncertainty, the mass emission rate measured with the dilution sampler is the same as that measured with the hot filter sample. Therefore, the magnitude of the gas-to-particle conversion occurring within the tunnel such as the previously discussed condensation and nucleation of sulfuric acid does not significantly affect the mass emission rate.

Table 2: Average $PM_{2.5}$ mass emission rates measure before and after the bag house.

	Mass Emissions (g/MBTU)	
	Before Baghouse	After Baghouse
Dilution Sampling	164 +/- 41	31 +/- 7
Hot Filter Sampling	176 +/- 28	23 +/- 18

Dilution and $PM_{2.5}$ Composition:

Enrichment factors are shown in Figure 9 to examine the effects of dilution sampling on $PM_{2.5}$ composition. Results are shown for three sets of experiments: Prater Creek Coal before the bag house, Prater Creek Coal after the bag house, and the blend of Prater Creek coal with wood pallets measured after the bag house. The results shown in Figure 9 are the average enrichment factors across all of the experiments for a given fuel and sampling location regardless of residence time or dilution ratio.

Figure 9 indicates that the majority of species have an enrichment factor of one indicating that the mass fraction of the species in the diluted sample is the same as that in the hot sample. For example, magnesium, calcium and lead are measured in equal amounts with hot and dilution sampling, regardless of fuel type, or sampling location (before or after the bag house).

Figure 9 indicates that selenium, ammonium and sulfate are enriched in the diluted samples. Selenium shows the greatest enrichment, with levels in the diluted sampling being as much as a factor of 12 than in the hot filters. The enrichment of selenium is not unexpected as it is known to be in the gas phase at stack conditions (Germani and Zoller 1988; Galbreath, Toman et al. 2000; Yan, Gauthier et al. 2001). In addition, enrichment of selenium has been observed in the plume downwind of a coal-fired power plant (Ondov et al. 1989). Since selenium is often used as a tracer for coal combustion in receptor models, it is important to understand the effects of sampling conditions on

selenium concentrations. These data indicate that hot filter sampling will underestimate selenium levels in $PM_{2.5}$.

Figures 10 and 11 examine the effect of dilution ratio and residence time on $PM_{2.5}$ mass factions of selenium, ammonium and sulfate -- the three species that show significant enrichment on Figure 9. In addition, $PM_{2.5}$ concentrations of one stable species, calcium, are shown for comparison.

Figure 10 plots the mass fractions of selenium, calcium, ammonium, and sulfate as a function of dilution ratio for the set of experiments performed before the bag house. Results from the hot filters are plotted at a dilution ratio of 1. The results for the diluted samples are averages of all the experiments conducted before the bag house at a given dilution ratio regardless of residence time. As expected, the mass fraction of calcium, a stable species, does not vary with dilution ratio. Selenium shows an enrichment factor of ~4 in the diluted sample. However, the enrichment of selenium does not vary with dilution ratio; for the conditions of these experiments a dilution ratio of 20 is sufficient to reduce the temperature of the exhaust to within 10 °C of ambient, assuming adiabatic mixing. Selenium is only present at trace levels in the emissions, so the amount gas-to-particle conversion indicated by this enrichment of selenium represents an insignificant amount of $PM_{2.5}$ mass (<0.05%) which is not enough to alter significantly the mass emission rate or changes in mass ratios of other species.

Figure 11 shows mass fractions of selenium, calcium, ammonium, and sulfate in $PM_{2.5}$ as a function of residence time for the set of experiments before the bag house. As expected, there is no trend in calcium levels with residence time. There are also no consistent trends in the concentration of the other species with residence time.

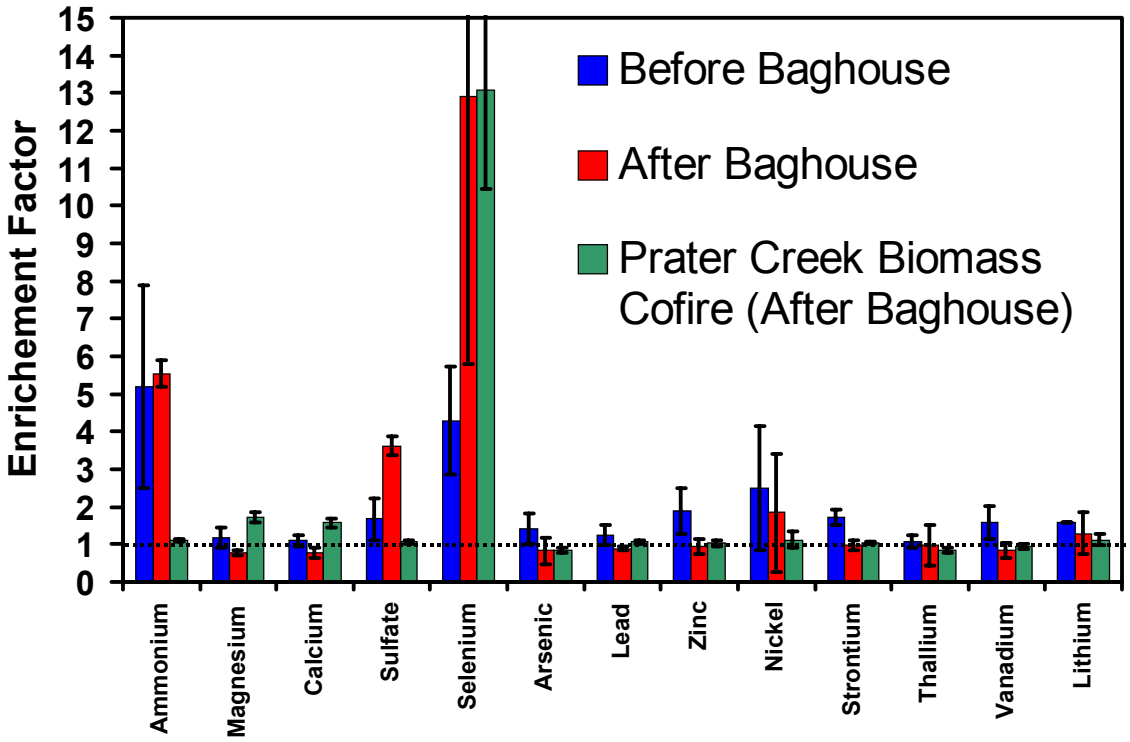

Figure 9: Average enrichment factors for a selection of trace species. Each case measured CERF emissions under the same conditions while firing Prater Creek Coal (one case cofired with biomass). Enrichment factors are based on the ratio between cold diluted samples and hot filter samples. Error bars are standard deviations.

The data in Figures 10 and 11 indicate that the $PM_{2.5}$ mass fraction of selenium in the diluted sample did not vary with dilution ratio or residence time; all that mattered was that the sample was diluted. Eatough et. al.(1996) reported high variability in selenium, arsenic, and lead emissions when dilution sampling, which they attributed to the gas-to-particle partitioning of these species not achieving equilibrium even at residence times as long as 30 minutes. The difference between results of these two studies may be due to different particle loadings in the exhaust. At the time of our experiments, the $PM_{2.5}$ emission rate from the CERF was a factor of 18 higher than the AP-42 emission factor for a coal source with a bag house firing a bituminous coal. Therefore the particle loadings and available surface area for condensation in the CERF exhaust are higher than stack conditions of a power plant operating with a more effective particulate control device. Since the condensation rate of selenium depends strongly on available surface area, gas-to-particle conversion may have occurred more rapidly in the CERF exhaust than what would occur under conditions with lower particle loadings. However, the results shown in Figure 11 indicate that even for the measurements made at the end of the tunnel (residence time of 0) the selenium levels in the $PM_{2.5}$ had reached there maximum and that condensation was complete.

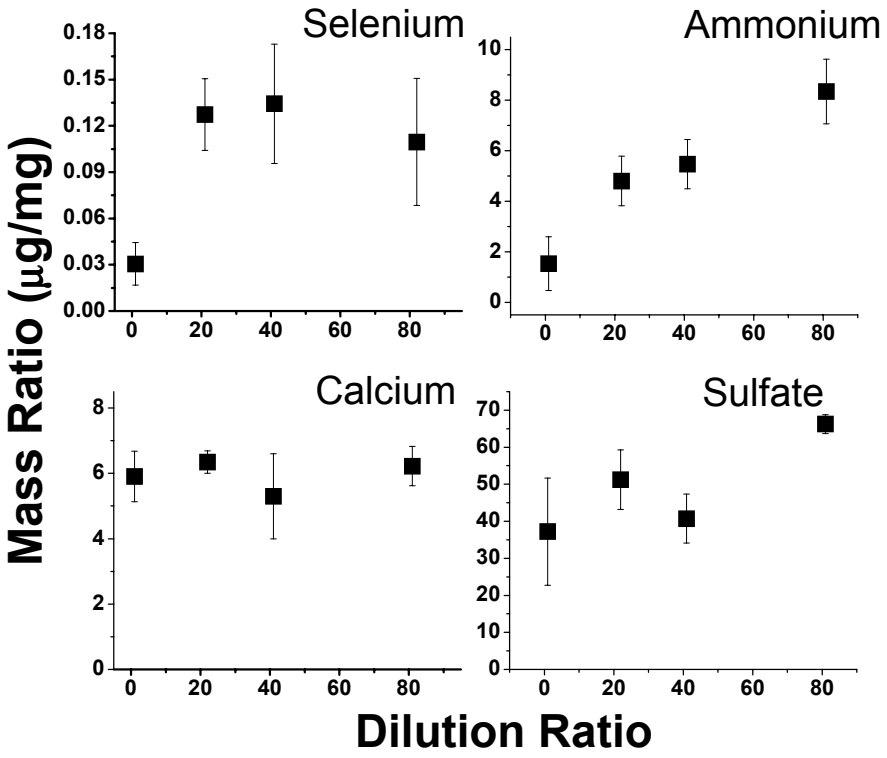

Figure 10: $PM_{2.5}$ mass fraction of selenium, ammonium, calcium, and sulfate as a function of dilution ratio. Results from hot filter samples are plotted at a dilution ratio of 1. Results are from before the bag house while firing Prater Creek coal. Error bars are standard deviations

For the experiments firing Prater Creek Coal, the $PM_{2.5}$ mass fraction of ammonium increased with dilution ratio (Figure 10), but did not vary with residence time (Figure 11). Enrichment is ammonium is likely due to gas-to-particle conversion of any ammonia gas in the system to neutralize the acidic aerosol. The linear increase in ammonium level with dilution ratio may be caused to the increased sampling times used at higher dilution ratios -- in order to collect the same amount of $PM_{2.5}$ mass on each filter, the sampling time was varied linearly with dilution ratio. However, the activated carbon bed on the dilution air inlet should remove ammonia, and ammonia emissions from coal combustors are low. Filter contamination is unlikely to cause the systematic trend in ammonium enrichment with dilution ratio shown in Figure 10. Finally, ammonium enrichment was not observed while firing the coal-wood blend (Figure 9) or the Black Thunder Coal suggesting that fuel composition also plays a role in ammonium enrichment. For these experiments the overall aerosol is not acidic.

The trends in sulfate level with dilution ratio (Figure 10) and residence time (Figure 11) are similar to ammonium. There is some increased enrichment at higher dilution ratio, and no trend with residence time. The sulfate enrichment could be a sampling artifact due to SO_2 reacting with species such as Ca on the filters. For these experiments

denuders were not used upstream of the filters. Again the increase in sulfate levels with dilution may be due to the longer sampling times at the higher dilution ratio.

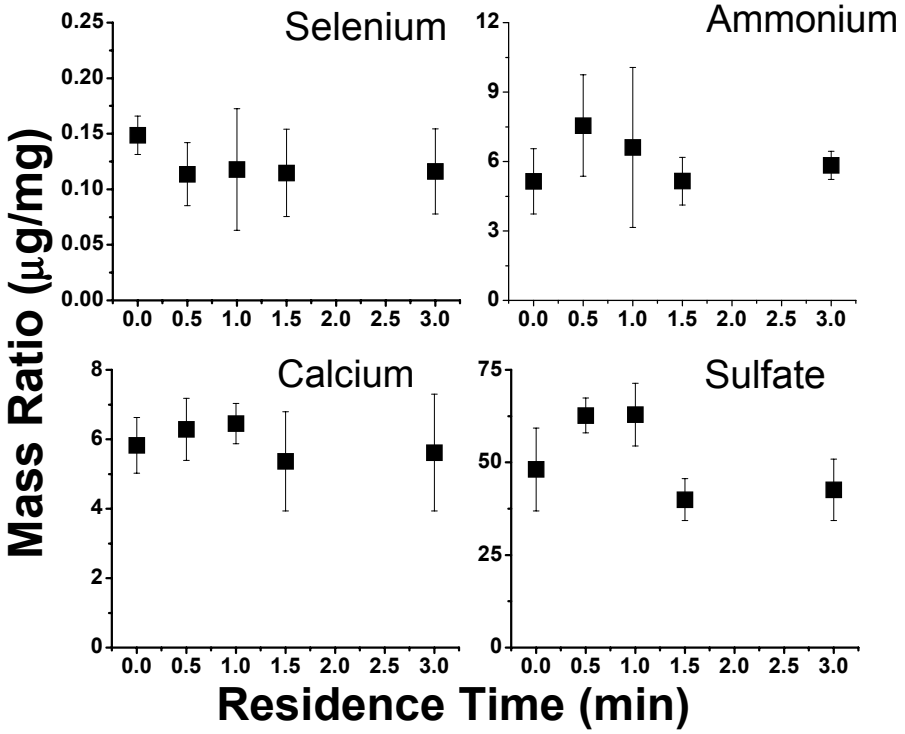

Figure 11: $PM_{2.5}$ mass fraction of selenium, ammonium, calcium, and sulfate as a function of dilution ratio. Error bars are standard deviations.

Figure 12 and Table 3 compares the $PM_{2.5}$ emission profiles for the experiments conducted while firing Prater Creek coal. The emission profiles measured before and after the bag house are comparable. Some significant differences can be seen in the emission profile of the unblended Prater Creek coal and the blend of Prater Creek Coal and wood, which illustrates the effects of variations in fuel ash composition on PM2.5 emissions. For example, the $PM_{2.5}$ emissions from the coal-wood blend have higher sodium, calcium and magnesium levels; these elements are all present at significantly higher levels in the wood ash than in the coal ash (Table 1). The ammonium level in the $PM_{2.5}$ emissions from firing unblended coal is significantly higher than the coal-wood blend.

Figure 13 and Table 3 compares the $PM_{2.5}$ emission profiles for three different coals: Prater Creek, Bailey Mine, and Black Thunder. Some of the differences between the emission profiles can be attributed to differences in fuel composition. For example, the higher $PM_{2.5}$ levels of calcium, magnesium and sodium in the emissions from Black Thunder Coal are consistent with the differences in ash composition shown in Table 1. Similarly, the Pittsburgh seam coal has the highest sulfur content and measured six times more sulfate than any other fuel's exhaust. These results clearly illustrate the effects that fuel composition has on the emissions, and how fuel analysis can serve as an indication on the composition of the emissions.

The emission profiles presented shown in Figure 13 are generally consistent with recent measurements by Watson et al. (2001) of $PM_{2.5}$ emissions from six commercial coal-fired boilers burning western coals. The differences are likely primarily due to differences in fuel composition and combustion conditions.

Emissions of organic and elemental carbon measured while firing Prater Creek Coal are listed in Table 3. Levels of OC and EC are low, contributing less than 5% of $PM_{2.5}$ mass in all cases. Watson et al. (2001) report a wide variation in OC and EC emissions from coal combustion, ranging from the low levels reported here OC and EC contributing as much as 34% and 8% of $PM_{2.5}$ mass. The large variability of OC and EC emissions is likely due to variations in combustion conditions potentially related to NOx control strategies.

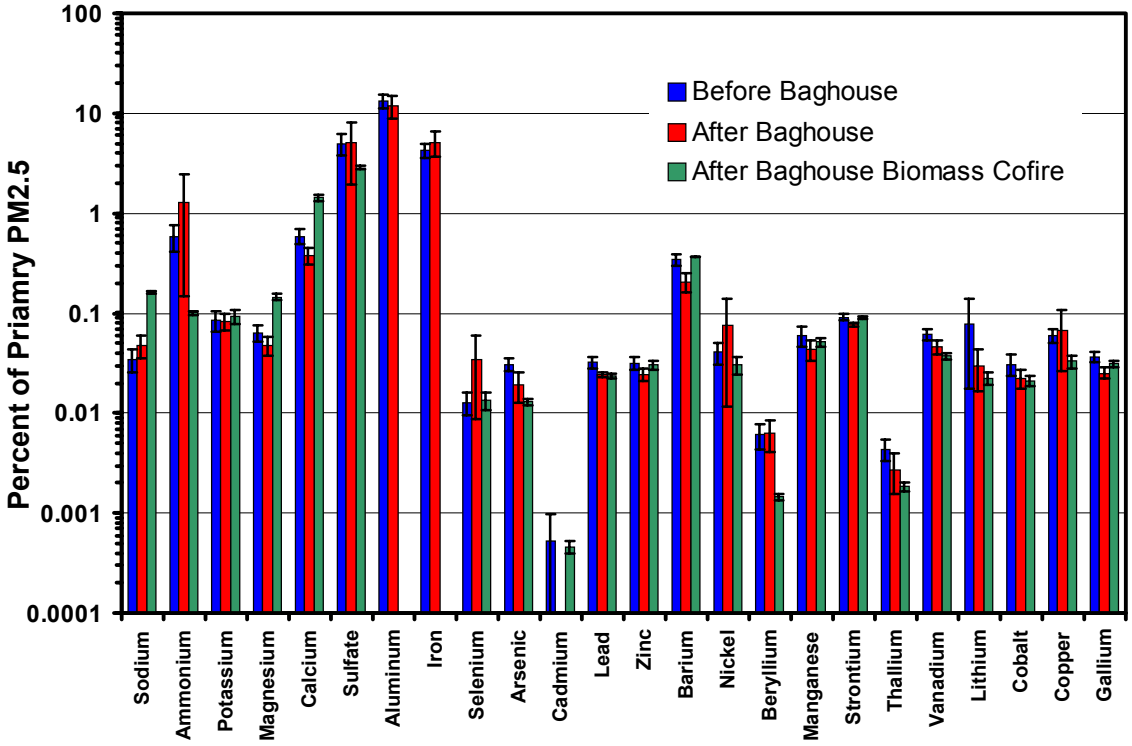

Figure 12: $PM_{2.5}$ Speciation Profiles for Prater Creek coal before and after the baghouse and Prater Creek cofired with biomass measured after the baghouse. The CERF was operated at the same nominal conditions while firing each fuel. Error bars are standard deviations.

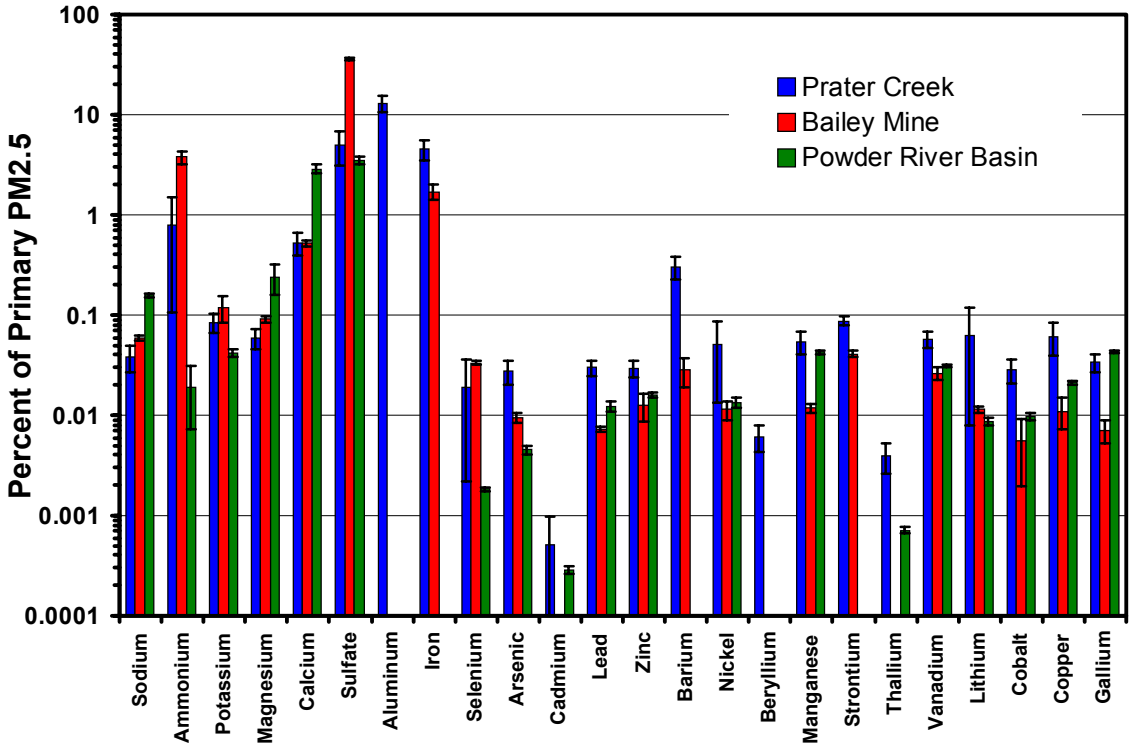

Figure 13: Speciation profiles for Prater Creek, Bailey Mine and Powder River Basin coals measured after the baghouse. The CERF was operated at the same nominal conditions while firing each fuel. Error bars are standard deviations.

Table 3: Chemical Speciation Profiles for different fuels while operating the CERF under the same conditions.

	Before Baghouse	After Baghouse			
Element	Prater Creek Coal	Prater Creek Coal	Prater Creek w/ Biomass	Powder River Basin	Bailey Mine
Sodium	0.03424 +/- 0.00870	0.04740 +/- 0.01199	0.16318 +/- 0.00546	0.15797 +/- 0.00635	0.05867 +/- 0.00357
Ammonium	0.58443 +/- 0.16858	1.3003 +/- 1.1529	0.10058 +/- 0.00360	0.01904 +/- 0.01172	3.7766 +/- 0.5411
Potassium	0.08562 +/- 0.01927	0.08350 +/- 0.01572	0.09369 +/- 0.01463	0.04196 +/- 0.00392	0.12044 +/- 0.03614
Magnesium	0.06363 +/- 0.01139	0.04753 +/- 0.01031	0.14615 +/- 0.01108	0.23925 +/- 0.07757	0.09062 +/- 0.00777
Calcium	0.58700 +/- 0.10055	0.37622 +/- 0.07188	1.4359 +/- 0.1007	2.8821 +/- 0.2925	0.52095 +/- 0.04459
Sulfate	4.9953 +/- 1.1781	5.0780 +/- 3.1271	2.8749 +/- 0.1079	3.5381 +/- 0.3138	36.169 +/- 1.108
Aluminum	13.3391 +/- 2.1160	11.8994 +/- 2.9731	n/a	n/a	n/a
Iron	4.27945 +/- 0.7181	5.1464 +/- 1.4179	n/a	n/a	1.7139 +/- 0.2996
Selenium	0.01266 +/- 0.00324	0.03477 +/- 0.02608	0.01344 +/- 0.00270	0.00184 +/- 0.00009	0.03346 +/- 0.00133
Arsenic	0.03080 +/- 0.00465	0.01928 +/- 0.00645	0.01303 +/- 0.00083	0.00454 +/- 0.00049	0.00951 +/- 0.00122
Cadmium	0.00052 +/- 0.00047	n/a	0.00046 +/- 0.00007	0.00028 +/- 0.00002	n/a
Lead	0.03256 +/- 0.00416	0.02407 +/- 0.00141	0.02359 +/- 0.00125	0.01241 +/- 0.00143	0.00730 +/- 0.00045
Zinc	0.031856 +/- 0.00453	0.02446 +/- 0.00365	0.03043 +/- 0.00293	0.01595 +/- 0.00094	0.01250 +/- 0.00384
Barium	0.34531 +/- 0.04641	0.20464 +/- 0.04301	0.36626 +/- 0.00310	n/a	0.02818 +/- 0.00946
Nickel	0.04046 +/- 0.00994	0.07604 +/- 0.06426	0.03050 +/- 0.00610	0.01353 +/- 0.00154	0.01145 +/- 0.00246
Beryllium	0.00610 +/- 0.00177	0.00629 +/- 0.00225	0.00146 +/- 0.00011	n/a	n/a
Manganese	0.05943 +/- 0.01340	0.04298 +/- 0.00993	0.05111 +/- 0.00476	0.04243 +/- 0.00183	0.01182 +/- 0.00113
Strontium	0.09121 +/- 0.00726	0.07776 +/- 0.00349	0.09018 +/- 0.00252	n/a	0.04075 +/- 0.00294
Thallium	0.00439 +/- 0.00110	0.00275 +/- 0.00118	0.00183 +/- 0.00017	0.00071 +/- 0.00005	n/a
Vanadium	0.06167 +/- 0.00856	0.04604 +/- 0.00756	0.03742 +/- 0.00265	0.03122 +/- 0.00121	0.02619 +/- 0.00375
Lithium	0.07810 +/- 0.06053	0.02983 +/- 0.01330	0.02248 +/- 0.00314	0.00863 +/- 0.00079	0.01142 +/- 0.00070
Cobalt	0.03097 +/- 0.00732	0.02250 +/- 0.00472	0.02099 +/- 0.00231	0.00967 +/- 0.00084	0.00559 +/- 0.00363
Copper	0.05956 +/- 0.00973	0.06676 +/- 0.04026	0.03311 +/- 0.00466	0.02105 +/- 0.00094	0.01104 +/- 0.00383
Gallium	0.03681 +/- 0.00418	0.02532 +/- 0.00341	0.03117 +/- 0.00269	0.04348 +/- 0.00132	0.00708 +/- 0.00187
OC	2.55 +/- 1.94	1.00	n/a	n/a	n/a
EC	0.85 +/- 0.25	4.90	n/a	n/a	n/a

Conclusions

This report examines the effects of residence time and dilution rate on fine particulate emissions from pulverized coal combustion. Particle size distributions were measured and filter samples were collected using a dilution sampler before and after the bag house of a pilot-scale pulverized coal combustor. Experiments were performed to examine the influence of dilution ratio and residence time on the size distribution and the total number and mass emissions. Filter samples were collected for speciation analysis to determine the effects of sampling conditions on $PM_{2.5}$ composition and mass emission rates.

For the samples collected before bag house, both dilution ratio and residence time strongly affected measurements of the particle size distribution. Coagulation is important before the bag house, shifting the size distribution to larger sizes and reducing the total number with increasing residence time. The occurrence of nucleation was a strong function of dilution ratio before the bag house, and the observed trends were consistent with theory. Nucleation was not observed at low dilution ratios because of the large amount of available surface area. Increasing the dilution ratio decreases the available surface area, slowing condensation, which allows nucleation to occur.

For the samples collected after the bag house, the dilution ratio and residence time did not affect the particle size distribution. Coagulation was not important because the particle concentrations are too low. Virtually no nucleation was observed after the bag house. Theory indicates that the lower particle concentrations after the bag house create conditions that are conducive to nucleation. The absence of nucleation was likely due to the removal of SO_3 from the flue gas in the bag house.

The $PM_{2.5}$ mass emission rate measured while dilution sampling agreed with that measured with a hot filter sample. Dilution did increase the mass fraction of selenium ammonium and sulfate in the $PM_{2.5}$ (these enrichments were not significant to increase the overall $PM_{2.5}$ mass emission rate within the experimental uncertainty). Selenium enrichment did not vary with dilution ratio and residence time.

A comparison of the emission profiles for each of the fuels tested show that differences in the profiles could be related to the ash composition of each fuel. Elements such as calcium, magnesium, and sodium, are found in higher concentrations in $PM_{2.5}$ formed while firing the Powder River Basin coal and the coal-wood cofire blend compared to the other fuels tested because of difference in fuel composition.

References

Abdul-Khalek, I., D. B. Kittelson, et al. (1999). SAE Technol. Pap. Ser. **No. 1999-01-1142**: 563-571.

Builtjes, P. J. H. and A. M. Talmon (1987). "Macroscale and Microscale Mixing in Chemical Reactive Plumes." Boundary-Layer Meteorology **41**(1-4): 417-426.

Cantrell, B. K. and K. T. Whitby (1978). "Aerosol Size Distributions and Aerosol Volume Formation for a Coal-Fired Power-Plant Plume." Atmospheric Environment **12**(1-3): 323-333.

Corio, L. A. and J. Sherwell (2000). "In-stack condensible particulate matter measurements and issues." Journal of the Air & Waste Management Association **50**(2): 207-218.

Damle, A. S., D. S. Ensor, et al. (1984). "Prediction of the Opacity of Detached Plumes Formed by Condensation of Vapors." Atmospheric Environment **18**(2): 435-444.

Eatough, D. J., M. Eatough, et al. (1996). "Apportionment of sulfur oxides at Canyonlands during the winter of 1990 .1. Study design and particulate chemical composition." Atmospheric Environment **30**(2): 269-281.

Eatough, D. J., M. Eatough, et al. (1996). "Apportionment of sulfur oxides at Canyonlands during the winter of 1990 .2. Fingerprints of emissions from point and regional sources impacting Canyonlands." Atmospheric Environment **30**(2): 283-294.

England, G., B. Toby, et al. (1998). Critical review of source sampling and analysis methodologies for characterizing organic aerosol and final particulate source emission profiles. Washington DC, American Petroleum Institute.

Flagan, R. C. and J. H. Seinfeld (1988). Fundamentals of Air Pollution Engineering. Englewood Cliffs, NJ, Prentice Hall.

Galbreath, K. C., D. L. Toman, et al. (2000). "Trace element partitioning and transformations during combustion of bituminous and subbituminous U. S. coals in a 7-kW combustion system." Energy & Fuels **14**(6): 1265-1279.

Germani, M. S. and W. H. Zoller (1988). "Vapor-Phase Concentrations of Arsenic, Selenium, Bromine, Iodine, and Mercury in the Stack of a Coal-Fired Power-Plant." Environmental Science & Technology **22**(9): 1079-1085.

Gillani, N. V., S. Kohli, et al. (1981). "Gas-to-Particle Conversion of Sulfur in Power-Plant Plumes .1. Parametrization of the Conversion Rate for Dry, Moderately Polluted Ambient Conditions." Atmospheric Environment **15**(10-1): 2293-2313.

Hildemann, L. M., G. R. Cass, et al. (1989). "A Dilution Stack Sampler for Collection of Organic Aerosol Emissions - Design, Characterization and Field-Tests." Aerosol Science and Technology **10**(1): 193-204.

Kauppinen, E. I. and T. A. Pakkanen (1990). "Coal Combustion Aerosols - a Field-Study." Environmental Science & Technology **24**(12): 1811-1818.

Kerminen, V. M. and A. S. Wexler (1995). "The Interdependence of Aerosol Processes and Mixing in Point- Source Plumes." Atmospheric Environment **29**(3): 361-375.

Kim, D. S., P. K. Hopke, et al. (1989). "Comparison of Particles Taken from the Esp and Plume of a Coal- Fired Power-Plant with Background Aerosol-Particles." Atmospheric Environment **23**(1): 81-84.

Lighty, J. S., J. M. Veranth, et al. (2000). "Combustion aerosols: Factors governing their size and composition and implications to human health." Journal of the Air & Waste Management Association **50**(9): 1565-1618.

Linak, W. P. and J. O. L. Wendt (1994). "Trace-Metal Transformation Mechanisms During Coal Combustion." Fuel Processing Technology **39**(1-3): 173-198.

Lipsky, E., C. O. Stanier, et al. (2002). "Effects of sampling conditions on the size distribution of fine particulate matter emitted from a pilot-scale pulverized-coal combustor." Energy & Fuels **16**(2): 302-310.

Luria, M., K. J. Olszyna, et al. (1983). "The Atmospheric Oxidation of Flue-Gases from a Coal-Fired Power-Plant - a Comparison between Smog Chamber and Airborne Plume Sampling." Journal of the Air Pollution Control Association **33**(5): 483-487.

Markowski, G. R., D. S. Ensor, et al. (1980). "A Sub-Micron Aerosol Mode in Flue-Gas from a Pulverized Coal Utility Boiler." Environmental Science & Technology **14**(11): 1400-1402.

Markowski, G. R. and R. Filby (1985). "Trace-Element Concentration as a Function of Particle-Size in Fly-Ash from a Pulverized Coal Utility Boiler." Environmental Science & Technology **19**(9): 796-804.

McElroy, M. W., R. C. Carr, et al. (1982). "Size Distribution of Fine Particles from Coal Combustion." Science **215**(4528): 13-19.

Meng, R. Z., P. Karamchandani, et al. (2000). "Simulation of stack plume opacity." Journal of the Air & Waste Management Association **50**(5): 869-874.

Mueller, S. F. and R. E. Imhoff (1994). "Estimates of Particle Formation and Growth in Coal-Fired Boiler Exhaust .1. Observations." Atmospheric Environment **28**(4): 595-602.

Mueller, S. F. and R. E. Imhoff (1994). "Estimates of Particle Formation and Growth in Coal-Fired Boiler Exhaust .2. Theory and Model Simulations." Atmospheric Environment **28**(4): 603-610.

Olmez, I., A. E. Sheffield, et al. (1988). "Compositions of Particles from Selected Sources in Philadelphia for Receptor Modeling Applications." Japca-the International Journal of Air Pollution Control and Hazardous Waste Management **38**(11): 1392-1402.

Ondov, J. M., C. E. Choquette, et al. (1989). "Atmospheric Behavior of Trace-Elements on Particles Emitted from a Coal-Fired Power-Plant." Atmospheric Environment **23**(10): 2193-2204.

Pinto, J. P., R. K. Stevens, et al. (1998). "Czech air quality monitoring and receptor modeling study." Environmental Science & Technology **32**(7): 843-854.

Querol, X., J. L. Fernandezturiel, et al. (1995). "Trace-Elements in Coal and Their Behavior During Combustion in a Large Power-Station." Fuel **74**(3): 331-343.

Seinfeld, J. H. and S. N. Pandis (1998). Atmospheric chemistry and physics: From air pollution to climate change. New York, John Wiley & Sons Inc.

Vandingenen, R. and F. Raes (1991). "Determination of the Condensation Accommodation Coefficient of Sulfuric-Acid on Water-Sulfuric Acid Aerosol." Aerosol Science and Technology **15**(2): 93-106.

Watson, J. G., J. C. Chow, et al. (2001). "PM2.5 chemical source profiles for vehicle exhaust, vegetative burning, geological material, and coal burning in Northwestern Colorado during 1995." Chemosphere **43**(8): 1141-1151.

Wehner, B., T. C. Bond, et al. (1999). "Climate-relevant particulate emission characteristics of a coal fired heating plant." Environmental Science & Technology **33**(21): 3881-3886.

Whitby, K. T., B. K. Cantrell, et al. (1978). "Nuclei Formation Rates in a Coal-Fired Power-Plant Plume." Atmospheric Environment **12**(1-3): 313-321.

Yan, R., D. Gauthier, et al. (2001). "Fate of selenium in coal combustion: Volatilization and speciation in the flue gas." Environmental Science & Technology **35**(7): 1406-1410.